

**Design analysis for thermoforming of thermoplastic composites  
Prediction and machine learning-based optimization**

Nardi, Davide; Sinke, Jos

**DOI**

[10.1016/j.jcomc.2021.100126](https://doi.org/10.1016/j.jcomc.2021.100126)

**Publication date**

2021

**Document Version**

Final published version

**Published in**

Composites Part C: Open Access

**Citation (APA)**

Nardi, D., & Sinke, J. (2021). Design analysis for thermoforming of thermoplastic composites: Prediction and machine learning-based optimization. *Composites Part C: Open Access*, 5, Article 100126. <https://doi.org/10.1016/j.jcomc.2021.100126>

**Important note**

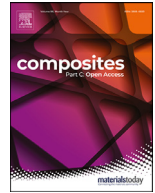
To cite this publication, please use the final published version (if applicable).  
Please check the document version above.

**Copyright**

Other than for strictly personal use, it is not permitted to download, forward or distribute the text or part of it, without the consent of the author(s) and/or copyright holder(s), unless the work is under an open content license such as Creative Commons.

**Takedown policy**

Please contact us and provide details if you believe this document breaches copyrights.  
We will remove access to the work immediately and investigate your claim.



# Design analysis for thermoforming of thermoplastic composites: prediction and machine learning-based optimization

Davide Nardi\*, Jos Sinke

Aerospace Manufacturing Technologies, Department of Aerospace Engineering, Delft University of Technology, Delft, Netherlands



## ARTICLE INFO

### Keywords:

Machine learning  
Manufacturing  
Analytical solutions  
Finite element analysis

## ABSTRACT

The correct prediction of a composite parts' final performance is of paramount importance during the initial design phase of the manufacturing process. To this end the correct evaluation of the most effective process parameters and their influence on the parts performance is key for the success of the manufacturing process. Our aim with this paper is to provide methodologies for the prediction of the temperature field in thermoplastic composites during thermoforming and to propose a strategy for process parameter selection. We measured the temperature variations over the different thermoforming stages and compared these values with analytical and finite element results. Our results show the accuracy of the predictions and the importance of the correct laminate temperature with respect to the prediction of the parts' spring-in angle. We discuss the essential features needed for accurate predictions of the temperature fields over the whole thermoforming process at an early design stage and the potential of a Machine Learning procedure based on Artificial Neural Network to aim for the optimum range of process parameters for a desired part performance outcome. In conclusion, we provide essential guidelines for blank temperature predictions, and the benefit of a machine learning-based tool over traditional approaches.

## 1. Introduction

Thermoforming of thermoplastic composites allows rapid transformation of flat laminates into the prescribed design by the combined action of heat and pressure [1,2].

The research conducted in thermoforming processes has been extensive, and mainly focused on the influence of the manufacturing process parameters on the resulting part characteristics. Table 1 lists some of the studies present in the literature.

The part development process starts typically with a conceptual design phase which results in the part manufacturing and testing. Unfortunately, such process is often iterative, and required design modifications are costly and time-consuming especially if deviations are detected at the final stages of the product development [19]. In fact, the variation of lay-up sequence, material, and processing parameters may introduce significant variability in terms of the expected part performances.

Predictions of thermoforming processes offered by finite element models (FEM) are useful to prevent trial and error testing so that robust and reliable process simulations can save costs and time during the initial design phase. Several deformation mechanisms take place during forming of composite laminates amongst which trellis shear, friction and bending are the most frequently implemented [20]. An overview of the studies on composite forming analysis can be found in [21]. However, FEM requires knowledge of the physical phenomena of the process, of

the material constitutive models and often times a high computational cost to obtain the required prediction is needed. A correct understanding of the influence of different process parameters is missing since thermoforming is a complex, nonlinear multivariable process in which understanding of the process parameters and of their interactions requires time-consuming experiments and simulations. Thus, there is a need for faster and more reliable approaches for the design phase of thermoforming of composites, so that final part characteristics, such as mechanical properties or void percentage, can be predicted with enough accuracy.

Recently, data-driven approaches based on machine learning (ML) techniques, such as Artificial Neural Network (ANN) have shown the potential to influence the design phase in the composites manufacturing industry [22] by means of detecting complex patterns relating the process and material input to the process outcome, e.g. porosity and mechanical properties of the laminate [23,24,25] and optimization [26]. This, especially in a design phase, can provide an effective tool to predict a specific output of the resulting composite, whereas the effects of the involved phenomena are yet fully understood. A review on ANNs applied to polymer composites can be found in [27].

The objective of our paper is to provide a supporting tool for the design phase of thermoplastic composites produced via thermoforming manufacturing. We focus on the prediction of the blank temperature over the process stages - blank heat-up in the heating stage, blank transport to the forming stage, and the blank forming - and the part spring-in

\* Corresponding author.

E-mail address: [D.Nardi@tudelft.nl](mailto:D.Nardi@tudelft.nl) (D. Nardi).

**Table 1**  
State of the art of the effect of the influence of process parameters on the part characteristics.

Authors (in alphabetical order)	Process parameters	Part characteristics
Barnes et al. [3]	Blank forming temperature, temperature-dependant material properties.	Residual stresses.
Chapman et al. [4]	Cooling rate, crystallization, relaxation time.	Residual stresses.
de Luca et al. [2]	Holding system, punch velocity, stacking sequence.	Ply wrinkling, fibre reorientation.
Dutta et al. [5]	Dwell time, forming pressure, mould temperature, forming time.	Thickness distribution, inner angles, voids, delaminations, fibre alignment.
Friedrich et al. [6]	Blank forming temperature, forming velocity, mould geometry.	Out-of-plane fibre buckling, in-plane fibre wrinkling, thickness distribution.
Han [7]	Layup configurations, mould temperature.	Spring-in angle.
Hou [8,9,10]	Die geometry, laminate dimension, blank forming temperature, mould temperature, forming pressure, holding time.	Part shape, tensile strength, fibre buckling, spring-in angle, void content, flexural mechanical properties.
Jain [11]	Mould temperature, blank forming temperature.	Void content, spring-in angle.
Jar [12]	Blank forming temperature.	Mode I and II delamination resistance.
Jeronimidis [13]	Blank forming temperature, temperature-dependant material properties.	Residual stress.
Lessard [14]	Preheating blank temperature, mould temperature, transfer time, stamping force.	Part thickness, interlaminar shear strength, degree of crystallinity.
McCool [15]	Blank forming temperature, mould temperature, consolidation compaction ratio.	Fibre volume fraction, surface roughness, manufacturing time, flexural strength, degree of crystallinity, cold crystallization temperature, reprocessing melt temperature.
O' Bradaigh [16]	Blank forming temperature.	Strength and stiffness.
Tatsuno [17]	Forming pressure, mould temperature.	Void content, process time.
Unger [18]	Cooling rate, annealing.	Residual stress.

(SI) angle induced upon cooling. The present work describes a holistic approach based on both analytical equations and FE simulations which can be effectively used to understand the effect of process and material variables on the evolution of the blank temperature field. In addition, a first attempt to use ANN in thermoforming manufacturing is presented, showing its potential as an effective tool for online monitoring and optimization of the thermoforming process.

The article is organized as follow. Section II presents the methodologies for the measurements and estimations of the temperature field of the consolidated laminate during the thermoforming stages. Section III reports the predicted temperature field obtaining via the previously described methodologies. Section IV is devoted to the discussion of the obtained results. Finally, section V concludes the article with conclusions and recommendations.

## 2. Methodology

### 2.1. General perspective

Since we aim at developing a comprehensive approach to predict the evolution of the temperature field during thermoforming processes, we do not limit our choice to a specific material. The selection we made was based on the available materials for the experimental tests and on the data present in the state-of-the-art.

For the heating stage we investigated the effect of different infra-red (IR) heater temperature and number of plies in the blank. We used (1) glass fibre reinforced polyetherimide (GF/PEI) woven composite 8 Harness Satin supplied by Toray and (2) carbon fibre reinforced polyamide 12 (CF/PA12) woven prepreg with twill weave supplied by Schappe Techniques. PEI is an amorphous polymer with a glass transition temperature ( $T_G$ ) of 217 °C and a processing temperature in the range of 320–350 °C. PA12 is a semi-crystalline polymer with a melting temperature of 176 °C and a processing temperature of 230 °C +/- 15 °C.

For the temperature evaluation during the transport stages and the temperature prediction during forming we used GF/PEI. For the prediction of the spring-in angle developing upon cooling we considered plain weave carbon fibre fabric reinforced polyetherimide (CF/PEI) from Ten Cate Advanced Composites.

Two thermocouples were placed at the top and at the bottom of the blank and temperatures were recorded by means of a Keithley Data Ac-

quisition device from the heating to the forming stages. We used both analytical equations and FEM to predict the recorded temperature during the experimental tests. We used FEM to predict the temperature during forming due to the complexity of the contact interaction between the blank and the forming dies.

Table 2 gives an overview of the adopted strategy for the blank temperature prediction for the thermoforming stages and the predictive approach employed.

Although the blank temperature plays a critical role for the part quality and mechanical performances, other process parameters, such as the forming pressure and the degree of cooling, can contribute to the optimization of the final component properties. Therefore, it is important to have a tool that can also take into account the variation of multiple input parameters at the early design stage. McCool et al. [15] considered three process control parameters for the thermoforming of carbon fibre/PPS thermoplastics laminate, namely the blank forming temperature, the mould tool temperature, and the mould tool consolidation compaction ratio (CCR), which describes the ratio of the nominal closed tool thickness over the nominal raw material thickness. They identified an optimal window for processing the part, along with the effect that the process parameters selection had on seven final characteristics of the manufactured parts, namely the variation of fibre volume fraction, the variation of surface roughness, the flexural strength, the degree of crystallinity, the cold crystallization temperature, and the reprocessing melt temperature. We used the results reported in [15] to evaluate the effectiveness of the ANNs for thermoforming manufacturing optimization in terms of the identification of the optimal processing parameters window. The comparison with the results obtained by [15] will be discussed in the following section, along with the potential that our approach has for both the early design stage and for inline process monitoring.

### 2.2. Experimental setup

The used experimental setup is shown in Fig. 1 and consists of:

- 21 ton pneumatic press;
- Rig with integrated infra-red (IR) oven, blank holder, shuttle transfer system and fume hood;
- Press assembly with integrated soft-hard tool set with an omega shape, and heating plate to keep the lower tool at a prescribed temperature.

**Table 2**  
Overview of the adopted strategy for the different stages.

Stage	Variable observed experimentally	Sampling time (s)	Material	Predictive approach
Heating	Temperature	5	GF/PEI	Analytical
		2	CF/PA12	
Transporting	Temperature	0.2	GF/PEI	Analytical
Forming	Temperature	10	GF/PEI	FEM
Cooling	Spring-in angle	/	CF/PEI	Analytical

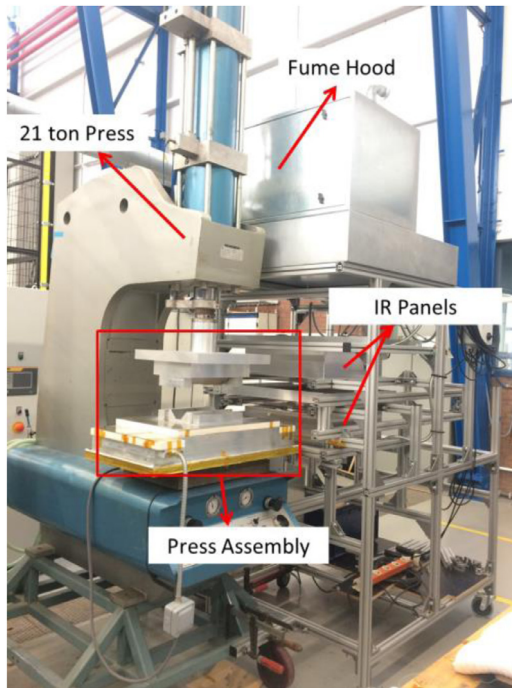


**Fig. 1.** Overview of the experimental setup [28].

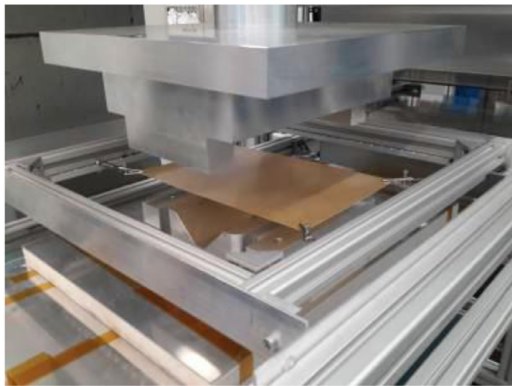


**Fig. 2.** Blank holder positioned in the press assembly [28].

A detailed report of the setup's sub-components can be found in [28].

The laminate is clamped using the blank holder (560 × 520) and positioned between the top and bottom IR lamps (500 × 500 mm). To ensure a uniform heating of the laminate, the IR lamps were placed at the same distance (150 mm) from the top and the bottom surface of the blank to prevent the blank sagging upon heating. A pneumatic cylinder was used to move the blank holder from the heating stage to the forming stage, which is represented in Fig. 2. Different volumetric flow rates (litre/minute) were considered to evaluate the difference in temperature drops resulting from the blank transport. The upper punch and the lower mould were 8 cm apart.

**Table 3**  
Material properties of GF/PEI and CF/PA12 laminates.

Material	GF/PEI	CF/PA12
Density, $\rho$ [Kg/m <sup>3</sup> ]	1910	1346
Thermal conductivity (through thickness), $k$ [W/m K]	0.4	5.66
Thickness, one ply [mm]	0.23	0.11
Specific heat, $C_p$ [J/Kg K]	890	1052

The use of a silicone rubber mould as the punch is preferred mainly due to the flexibility of the rubber which allows the adaptation to the laminate thicknesses. Aluminium was used for the hard mould. Maximum temperature for the aluminium when operating continuously was limited to 220 °C, a value that the rubber could also withstand.

### 2.3. Prediction of the temperature field

#### 2.3.1. Heating up stage

We consider the following assumptions for the heat transfer problem [29]: (i) heat convection and radiation occur only in the thickness direction (no heat transfer around the edges), (ii) the thermal conductivity  $k$  is isotropic, (iii) the ratio  $k/\rho C_p$  is temperature independent, where  $\rho$  is the density, and  $C_p$  is the specific heat of the blank materials, (iii) linearization of the thermal boundary conditions is acceptable.

We use a coordinate system with the origin at the centre of the blank having the  $z$ -axis perpendicular to the blank plane. The governing differential equation for the heat conduction is

$$\frac{\partial}{\partial z} \left[ k \frac{\partial T}{\partial z} \right] = \rho C_p \frac{\partial T}{\partial t} \quad (1)$$

The general solution for the temperature variation at the centre of the blank ( $z = 0$ ) becomes

$$T_h(0, t) = T_{IR} - (T_{IR} - T_0) \sum_{n=1}^{\infty} \frac{4 \sin \lambda_n}{2\lambda_n + \sin 2\lambda_n} \exp\left(\frac{-\lambda_n k t}{\rho C_p a^2}\right) \quad (2)$$

where  $T_{IR}$  is the heater temperature,  $T_0$  the initial blank temperature,  $t$  the elapsed time,  $a$  the half thickness of the blank, and  $\lambda_n$  are the roots of the equation

$$\lambda_n \tan \lambda_n - \frac{h_h a}{k} = 0 \quad (3)$$

with  $h_h$  the heat transfer coefficient for heating. To solve Eq. (3) we use the values reported in Appendix B3 [30] selecting the  $\lambda_n$  in a range that would best fit the experimental data. The selected  $\lambda_n$  is associated to a reported value of the Biot number (Bi) defined as

$$Bi = \frac{h_h a}{k} \quad (4)$$

From Eq. (4) the  $h_h$  value can be finally computed.

The material properties required to compute Eq. (2) are reported in Table 3. We used the material properties at room temperature. For GF/PEI these properties were given in [31], except for the density which is provided in the product data sheet [32]. For CF/PA12 no material data were available from the supplier, except for the thickness [33]. Wakeman et al. [34] used CF/PA12 provide by the same supplier and they reported a fibre volume fraction of 56%. We collect the data on the

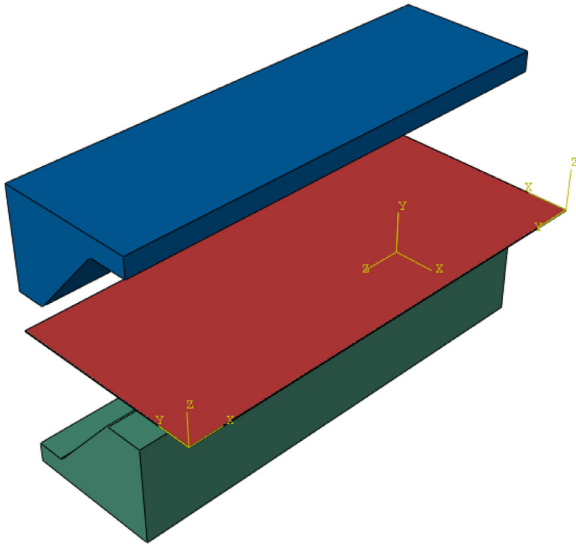


Fig. 3. Components of the FEM model in ABAQUS: mould (green), blank (red) and punch (blue). (For interpretation of the references to colour in this figure legend, the reader is referred to the web version of this article.)

PA12 from [35] and we assume the use of T-300 carbon fibre [36]. We then performed a rule-of-mixture assessment to compute the material properties of the CF/PA12 laminate reported in Table 3.

2.3.2. Transporting stage

Similarly, the temperature variation at the centre of the blank ( $z = 0$ ) during the transporting stage ( $T_t$ ) can be expressed as

$$T_t(0, t) = T_{IR} - (T_{IR} - T_h) \sum_{m=1}^{\infty} \frac{4 \sin \lambda_m}{2\lambda_m + \sin 2\lambda_m} \exp\left(\frac{\lambda_m kt}{\rho C_p a^2}\right) \quad (5)$$

where  $\lambda_m$  are the roots of the equation

$$\lambda_m \tan \lambda_m - \frac{h_c a}{k} = 0 \quad (6)$$

and  $h_c$  is the heat transfer coefficient for cooling,  $T_h$  is the temperature at the end of the heat-up stage and the other variables are the same considered in Eq. (1). We considered a [(0/90)(90/0)] blank of GF/PEI material heated at 320 °C and then moved this blank to the forming stage with a pneumatic actuator [37] with a prescribed volumetric flow rate of 50 L/min.

2.3.3. Forming stage

We performed a thermoforming test on a [(0/90)(90/0)] GF/PEI laminate heated to 320 °C. We set the mould at 220 °C, just above the  $T_G$  of PEI, while the we kept the punch at room temperature since no heating mechanisms was available for the upper tool. We set the pressure of the punch actuator so that the punch would descend at a speed of 4 mm/s. The forming step had a duration of approximately 220 s.

We developed a finite element model in ABAQUS/Standard to predict the blank temperature field at the moment of closing of the mould. Fig. 3 shows the components of the FE model with different colours representing the mould, the die and the punch, respectively in green, red and blue. Half of the geometries are considered due to the symmetry of the problem. Symmetry boundary conditions on the displacements were applied on the left side of the components. The mould was constrained in all the six degrees of freedom and the punch too, except for the vertical translation to allow the descending towards the mould. The laminate was fixed on the right side allowing the translation in the vertical and lateral directions.

We employed a coupled structural/thermal analysis to simulate the displacement of the laminate towards the mould. We used 3D continuum elements (C3D8T) for both the blank and the tools. We modelled

each ply (0/90) as a single homogeneous solid. The orthotropic thermal properties as a function of the temperature were obtained from [31]. The orthotropic mechanical properties as a function of the temperature were not available in literature. Hence, we assumed the ones from CF/PEI presented in [11] (see Table 4) due to the lack of influence of the fibre material with respect to PEI for this kind of analysis.

The key features of the simulation were the thermal properties of the involved contacts, namely between the mould and the bottom ply, between the two (0/90) GF/PEI plies, and between the top ply and the punch. The thermal contact properties are formulated in terms of conductance ( $W/m^2K$ ) and clearance (m) [38]. We selected the values of the conductance and of the clearance that produced the best approximation with the experimental results.

2.3.4. Cooling stage

We used a predictive analytical model based on the classical lamination theory and we considered symmetric lay-ups subjected to a homogeneous change in temperature through the laminate thickness. The effect of viscoelasticity is considered by means of the variation of the elastic and thermal properties as a function of the  $T_G$  of the thermoplastic matrix. We focused on the resulting curved portion of the formed part since for a symmetric lay-up the straight portions will remain straight upon cooling if the cooling is uniformly. The effect of crystallinity is not considered.

The equation employed to compute the spring-in (SI) is [39]

$$SI = \Delta T \left( \epsilon_{2,T,P}^0 - \alpha_{Z,P} \right) \quad (7)$$

where

$\Delta T$  is the homogeneous temperature change along the laminate thickness,

$\epsilon_{2,T,P}^0$  is the second component of the strain of the middle surface,  $\alpha_{Z,P}$  is the average thermal expansion coefficient of a laminate perpendicular to the surface, computed as follow:

$$\alpha_{Z,P} = \frac{1}{h} \left[ \Delta h_T \left( \frac{h}{2} \right) - \Delta h_T \left( -\frac{h}{2} \right) \right] \quad (8)$$

where  $h$  is the laminate thickness, and  $\Delta h_T$  represents the thickening of the laminate which is the variation of the thickness due to the difference between the in-plane and out-of-plane strains in the plies which are due to the variation of temperature [40,41], computed as

$$\Delta h_T(z) = \int_0^z \alpha_z dz + \int_0^z S_n \sigma_T^x dz \quad (9)$$

where  $z$  is the coordinate normal to the surface,  $\alpha_z$  is the thermal expansion coefficient in the thickness direction,  $S_n$  is the normal component of the compliance tensor and  $\sigma_T^x$  is the vector representing the stress in the laminate due to the temperature change.

2.3.5. ANN for thermoforming of thermoplastic composites

ANN consists of many interconnected neurons in which one or more scalar inputs are multiplied by corresponding weights thus producing a sum of products that is used as input for a transfer function to produce a scalar output. In addition to the weights, a bias  $b$  is imposed to each neuron. Simply put, single neurons of such networks receive input signals and transform these input signals into output signals that are transmitted to the next neuron along the processing direction. The functions that determine the input-output behaviour are called 'transfer functions', i.e. activation functions and output functions. The transfer function may be chosen from a variety of available functions whose selection is based mostly on trial-and-error tests of the ANN performance and results from the literature [23,42].

The proposed methodology to predict one or more selected part characteristics is based on (i) data preparation, (ii) ANN model building and (iii) evaluation. In the first step all the available data relevant to the targeted aspect are gathered. We achieved this step considering data form the literature. Then we built the ANN model based on the training

**Table 4**  
Material properties of CF/PEI [11].

Property	$E_{11} = E_{22}$ [GPa]	$E_{33}$ [GPa]	$G_{12}$ [GPa]	$\nu_{12}$	$\nu_{13} = \nu_{23}$	$\alpha_1 = \alpha_2$ [ $\mu\epsilon/^\circ\text{C}$ ]	$\alpha_3$ [ $\mu\epsilon/^\circ\text{C}$ ]
Below $T_G$ ( $< 217^\circ\text{C}$ )	67	6	2.7	0.024	0.27	2.35	45.8
Above $T_G$ ( $\geq 217^\circ\text{C}$ )	67	6	2.7	0.024	0.27	2.35	59.7

**Table 5**  
Tests and process parameters overview [15].

Test	Blank forming temperature [ $^\circ\text{C}$ ]	Mould tool temperature [ $^\circ\text{C}$ ]	CCR
1	310	50	0.94
2	310	110	0.97
3	310	170	1.0
4	340	50	0.97
5	340	110	1.0
6	340	170	0.94
7	370	50	1.0
8	370	110	0.94
9	370	170	0.97

data selected from the available data from the previous step. Finally, a relationship between the set of independent variables, i.e. process and material parameters, and the targeted characteristics is inferred by applying the built relationship onto a new set of unseen data.

Tables 5 and 6 show the overview of the tests [15] based on the variation of three process parameters and the results in terms of the effect on seven part characteristics of CF/PPS laminates, respectively.

The authors conducted an analysis of means (ANOM) which allowed them to perform a series of virtual optimizations to predict the value of the characteristics of the final parts. The influence of the values of the process parameters within the chosen range, e.g. a blank forming temperature of  $330^\circ\text{C}$ , was assumed to follow a (piecewise) linear interpolant function, as shown in Fig. 4 where the ANOM results of the three process parameters on the flexural strength are reported.

We trained several ANNs considering the values reported in Tables 5 and 6 as input and output values for the models, respectively. To evaluate the performance of the ANNs we considered

- a) different data allocation (%) for: Training (T), Validation (V), Test (TT);
- b) hidden neurons number (HN).

Nine combinations resulted from the considered approach, as reported in Table 7.

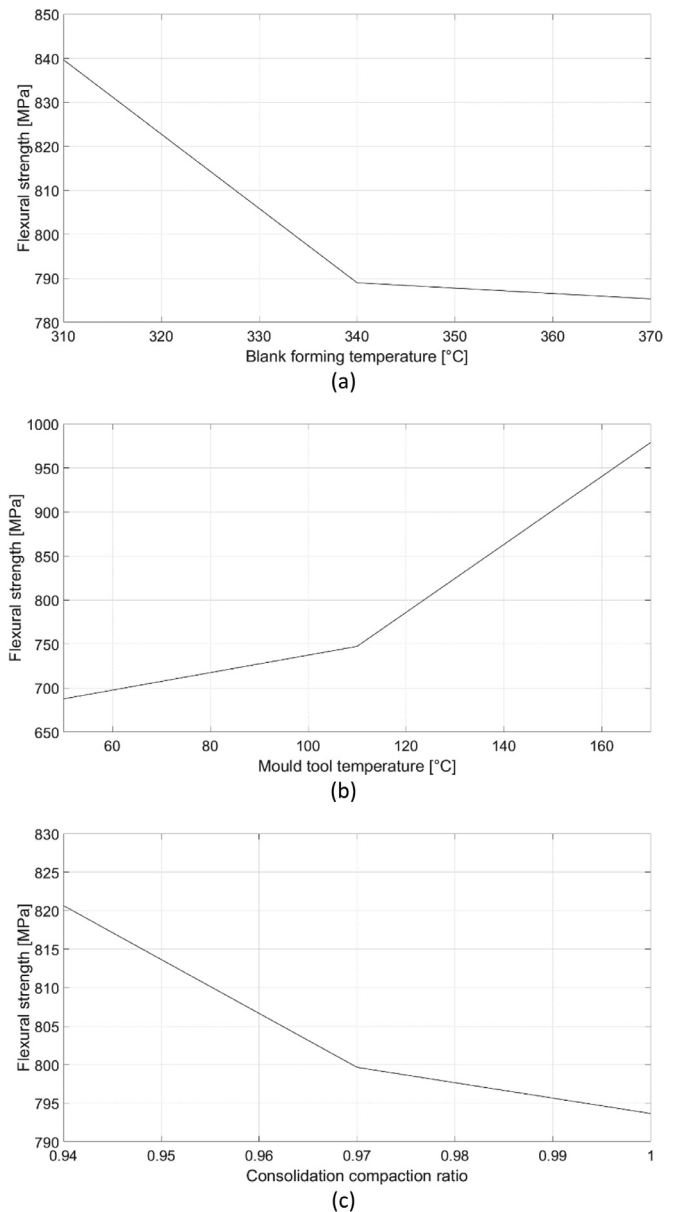
We initially considered the optimization of process parameters to obtain the best output for the flexural strength. Then, we discussed the influence of the data division and of the HN to obtain the best combination amongst the nine scenarios based on the comparison of the ANN models with the ANOM prediction performed by [15]. Lastly, we applied the best ANN model combination to the prediction of other three part characteristics, namely (a) the derived production cycle time, and of (b) the degree of crystallinity. Since the division of the data amongst the three different sets (T, V, TT) was randomly performed, the ANN was built five times for each scenario. For this investigation we used a Bayesian-Regularization and a sigmoid as training and transfer function, respectively. The influence of these functions on the predictive capability is beyond the scope of this work.

Table 8 summarizes the architecture of the considered ANN models.

### 3. Results

#### 3.1. Heating up stage

In the experimental tests we consider the influence of the following parameters on the evolution of the temperature field:



**Fig. 4.** ANOM for the effect of the blank forming temperature (a), the mould tool temperature (b), and the CCR (c) on the parts flexural strengths [15].

- 1 The influence of different IR heaters temperatures -  $300^\circ\text{C}$ ,  $400^\circ\text{C}$  and  $500^\circ\text{C}$  - for a [(0/90)(90/0)] GF/PEI consolidated blank.
- 2 The influence of plies number N - 2, 4 and 6 - for a (0/90)<sub>N</sub> CF/PA12 consolidated blank.

- Influence of IR heater temperature

Fig. 5 shows the temperature increase at the top of the blank during the heating up stage for the selected IR heaters temperatures. Firstly, a larger temperature trend variation can be seen when the IR heaters temperature was set at  $500^\circ\text{C}$  with respect to trends observed for IR

**Table 6**  
Results of the performed tests [15].

Test	Variation of fibre volume fraction [ $\Delta\%$ ]	Variation of Surface roughness [ $\Delta\mu\text{m}$ ]	Derived production cycle time [s]	Flexural Strength [MPa]	Degree of crystallinity [%]	Cold crystallization temperature [°C]	Reprocessing melt temperature [°C]
1	8.15	1.14	430	739	12.6	135	278
2	5.39	1.05	522	765	20.8	132	278
3	5.9	0.96	590	1015	29.4	113	280
4	7.2	1.56	458	679	11.4	137	277
5	7.07	1.58	533	721	12.5	137	279
6	4.49	1.48	604	967	20.9	114	277
7	5.11	1.16	483	645	8.9	134	275
8	4.1	1.49	554	756	14.1	138	274
9	5.81	1.18	624	955	20.8	114	274

**Table 7**  
Overview of the ANN-based investigation.

	T 70%V 15%TT 15%	T 70%V 25%TT 5%	T 50%V 25%TT 25%
HN 1	A	B	C
HN 5	D	E	F
HN 10	G	H	I

**Table 8**  
Architecture of the ANN models.

Hidden Layers number	1
Hidden Neurons number - Input	1/5/10
Hidden Neurons number - Output	3
Training Function	Bayesian-Regularization
Transfer Function	Sigmoid

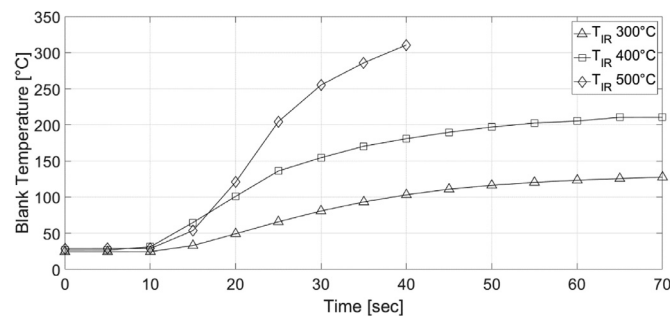


**Fig. 5.** Temperature variation at the top of the GF/PEI blank during the heat-up stage for prescribed IR heaters temperatures (300 °C, 400 °C and 500 °C).

temperatures of 300 °C and 400 °C. The heat transfer phenomena are complex and this might represent a possible reason for such temperature behaviour. Secondly, it can be seen that only when the temperature of the IR heaters was set at 500 °C the temperature of the blank increased above the PEI glass transition temperature of 217 °C. The reason can be found in the dominance of the heat losses with the environment over the provided heat. We hence focused our predictions only on the case of the IR heater temperature of 500 °C.

From Appendix B3 in [30] we chose the first root  $\lambda_1$  to solve the transcendental Eq. (3) that produced the best fit with the experimental data. This  $\lambda_1$  is 0.085. The resulting Biot number (Bi) is 0.0072. The computed heat transfer coefficient  $h_h$  is 12.5 W/m<sup>2</sup>K. Fig. 6 shows the comparison between the experimental data and the estimated values of the temperature profiles at the top of the blank using Eq. (2).

• Influence of plies number

We considered the heating of three blanks with 2, 4 and 6 plies, respectively, with a IR heaters temperature of 500 °C. Fig. 7 displays the three experimental temperature profiles. The measurements stopped at 250 °C which is the end of the processing temperature range for PA12.

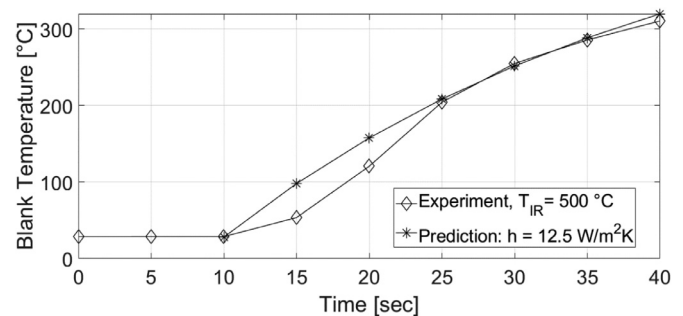


**Fig. 6.** Comparison of experimental ( $\diamond$ ) and estimated ( $*$ ,  $\circ$ ) temperature profiles at the top of the GF/PEI blank for the resulting heat transfer coefficient  $h = 12.5 \text{ W/m}^2\text{K}$ .

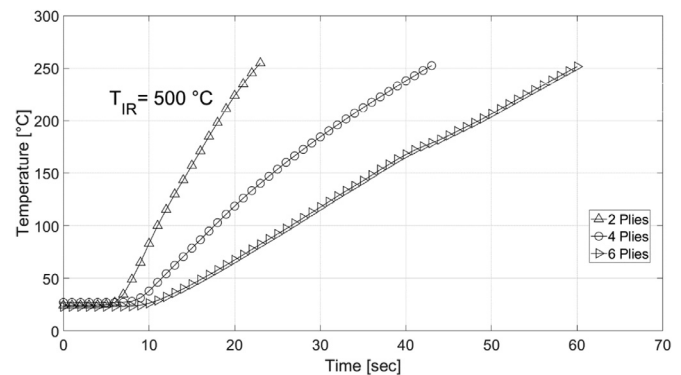


**Fig. 7.** Temperature variation at the top of the CF/PA12 blank during the heat-up stage for IR heaters at 500 °C for blanks with 2, 4, and 6 plies.

We used the same procedure based on [30] to estimate the solution of Eq. (3). Figs. 8–11 show the comparison between the experimental data and the estimated values of the temperature profiles at the top of the three considered blanks. The evaluation of the heat transfer coefficients via the previously described procedure led to values between 6 and 7.9 W/m<sup>2</sup>K.

3.2. Transporting stage

The temperature recorded from the top of the blank is reported in Fig. 11. It can be seen that after an initial plateau (0 - 0.7 s) due to the time lag between initializing the temperature recording and the actuation of the pneumatic actuator the blank temperature drops for about 45 °C in about 3 s before reaching a new plateau and starting again to drop with a lower rate. The trend is due to the fact that in the first 3 s the blank is moved towards the forming station without any insulation from the open environment. After 3 s the blank has reached the forming station with a lower mould temperature of 200 °C.

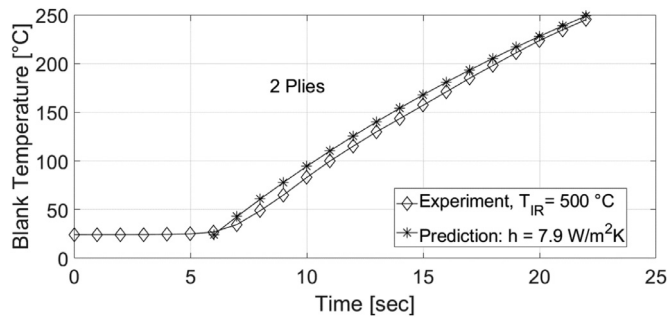


Fig. 8. Comparison of experimental ( $\diamond$ ) and estimated ( $*$ ,  $\circ$ ) temperature profiles at the top of the 2-ply CF/PA12 blank for the resulting heat transfer coefficient  $h = 7.9 \text{ W/m}^2\text{K}$ .

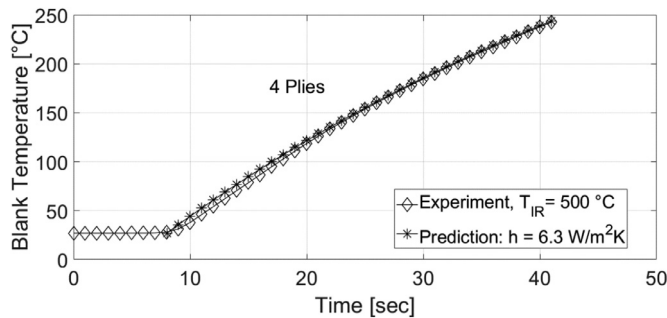


Fig. 9. Comparison of experimental ( $\diamond$ ) and estimated ( $*$ ,  $\circ$ ) temperature profiles at the top of the 4-ply CF/PA12 blank for the resulting heat transfer coefficient  $h = 6.3 \text{ W/m}^2\text{K}$ .

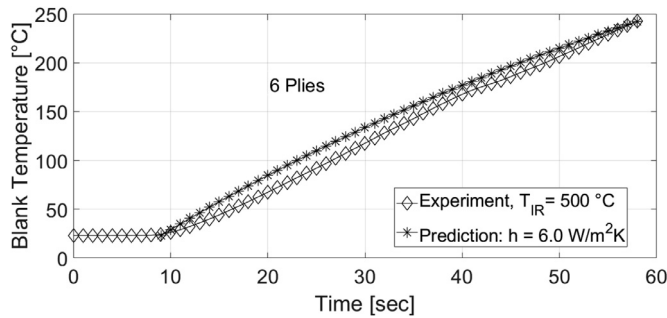


Fig. 10. Comparison of experimental ( $\diamond$ ) and estimated ( $*$ ,  $\circ$ ) temperature profiles at the top of the 6-ply CF/PA12 blank with the resulting heat transfer coefficient  $h = 6.0 \text{ W/m}^2\text{K}$ .

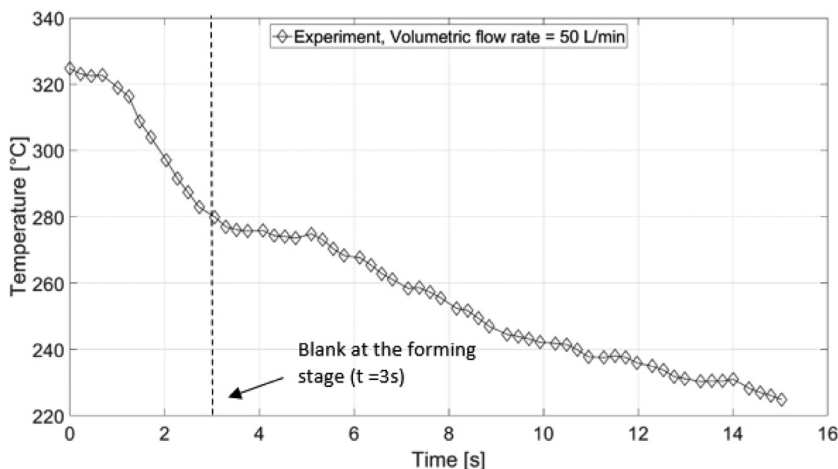


Fig. 11. Experimental temperature profile at the top of the 2-ply GF/PEI blank transported from the heating stage to the forming stage; volumetric flow rate 50 L/min.

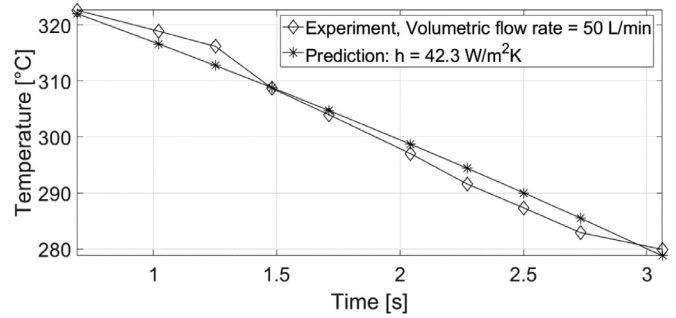


Fig. 12. Comparison of experimental ( $\diamond$ ) and estimated ( $*$ ) temperature profiles at the top of the 2-ply GF/PEI blank with the resulting heat transfer coefficient  $h = 42.3 \text{ W/m}^2\text{K}$ .

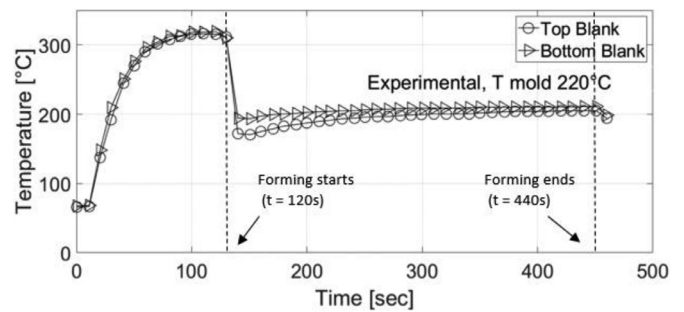


Fig. 13. Evolution of the temperature field at the top and bottom of the GF/PEI laminate during the thermoforming cycle test;  $T_{\text{mould}} = 220 \text{ }^\circ\text{C}$ .

To predict the temperature variation during forming we adopted the same procedure used for the heating up prediction now using Eq. (4). Fig. 12 shows the comparison between the experimental data and the estimated values of the temperature profiles at the top of the blank. The evaluation of the heat transfer coefficients via the previously described procedure led to  $42.3 \text{ W/m}^2\text{K}$ , a much higher value than that for the heating stage due to the movement of the blank.

### 3.3. Forming stage

Fig. 13 shows the temperature evolution at the top and at the bottom of the blank during the whole process, namely heating up the blank, transport and forming. Focusing on the forming step (starting at  $t = 120 \text{ s}$  and ending at  $t = 440 \text{ s}$ ), the top ply experiences a higher temperature drop than the bottom ply due to the contact with the punch at room temperature.

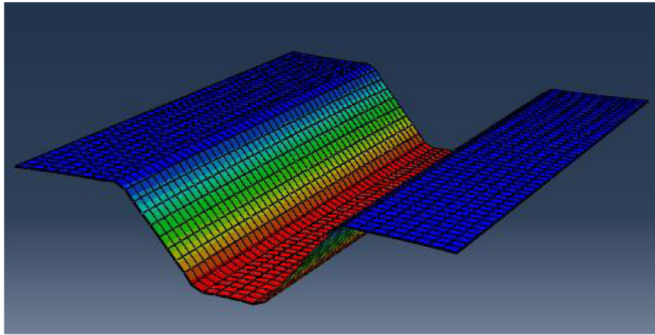


Fig. 14. Formed blank resulting from the FEA.

Table 9

Comparison between the temperature values at the forming stage of the experimental tests and the FEM; T mould = 220 °C.

Position	Experimental T [ °C]	Numerical T [ °C]	Variation (%)
Top	205	205	n.a.
Bottom	211	214	+ 1.4

perature. The temperature at the end of the forming stage was 211 °C and 205 °C at the bottom and at the top of the blank, respectively. In terms of blank manufacturing such test would not be appropriate since the blank temperature is below the T<sub>G</sub> of PEI. The modification of the setup conditions for a proper thermoforming process, such as both the mould and the punch made of steel to increase the allowable tools temperature, is not within the scope of our current work.

The conductive heat transfer between the contact surfaces is defined by [38]

$$q = k(\theta_A - \theta_B) \tag{10}$$

where q is the heat flux per unit area crossing the interface from point A on the first surface to point B on the other,  $\theta_A$  and  $\theta_b$  are the temperatures of the points on the surfaces, and k is the gap conductance, which is also dependant on the clearance between A and B, where a clearance equal to zero means that the gap is closed, i.e. the two surfaces are in contact. are

The values of the gap conductance and of the gap clearance for the modelled contacts played a major role in the prediction accuracy. For simplicity, we kept the gap clearance fixed to 0.1 for all the contacts and then we varied the gap conductance value. The gap conductance values for the involved contacts were tuned so that the temperature at the top of the blank was the same of the temperature resulted from the experimental test.

Fig. 14 shows the FEA of the resulting laminate after the forming stage, in which the colour represents the magnitude of the vertical displacement. Based on this simulation, the nodes in the centre of the blank on top and on bottom were evaluated in terms of their temperature variation.

Table 9 reports the experimental and numerical values of the temperature for the top and the bottom surfaces of the blank with the relative variation (%).

The gap conductance values that gave the best fit are reported in Table 10. It can be seen that even if those values were obtained to fit the numerical results they still retain a physical meaning. In fact, a lower value of the gap conductance represents a higher value of thermal resistivity. Hence, it is reasonable to expect a higher value of gap conductance between the plies, where ideally the contact between the layers is perfect, a lower value of gap conductance between the top ply and the punch, where the heat absorption capability of the rubber mould is poor, and an intermediate gap conductance value for the contact between the bottom ply and the aluminium mould.

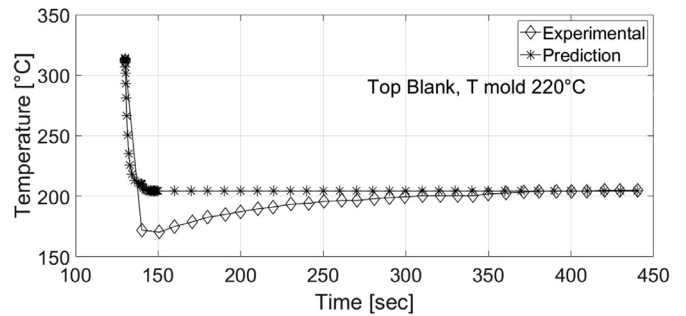


Fig. 15. Comparison between the experimental (◇) and estimated (\*) temperature values during forming at the top of the blank; T mould 220 °C.

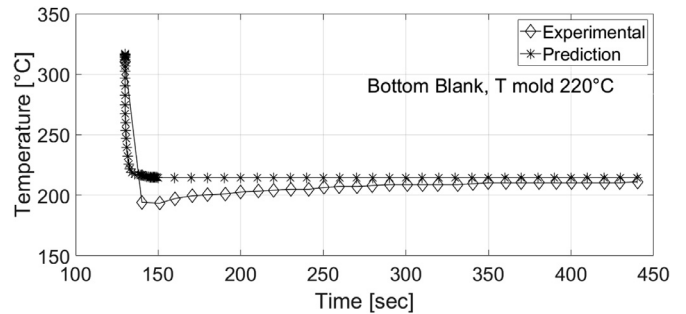


Fig. 16. Comparison between the experimental (◇) and estimated (\*) temperature values during forming at the bottom of the blank; T mould 220 °C.

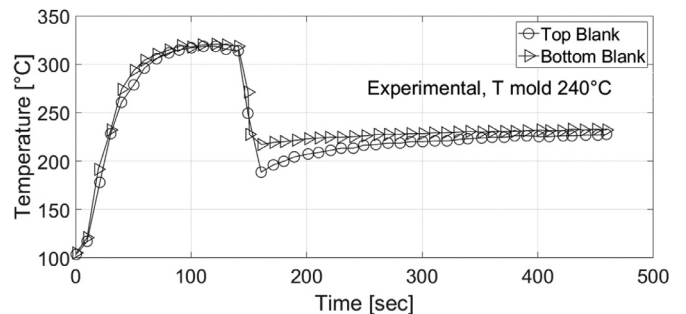


Fig. 17. Evolution of the experimental temperature field at the top and bottom of the GF/PEI laminate during the thermoforming cycle test; T mould = 240 °C.

Figs. 15 and 16 show the comparisons between the experimental and the estimated temperature profiles obtained via the FE analysis using the reported values of gap conductance for the top and the bottom surfaces of the blank, respectively. Only the forming stage was addressed in this simulation. For both top and bottom side of the blank a temperature drops well below the equilibrium temperature in the experimental tests at the very beginning of the forming step is recorded by the thermocouples. The drop is more notable for the top of the blank than for the bottom. This behaviour is related to the rubber punch that came in contact with the top blank which is much colder with respect to the mould. The blank temperature reaches its equilibrium at 205.5 °C and at 211.5 °C for the surfaces at the top and the bottom of the blank, respectively.

The equilibrium temperature at the top and at the bottom of the laminate predicted by the FEA is in good agreement with the experimental values. However, to validate the model, we performed an additional test in which the we set the mould temperature at 240 °C.

Fig. 17 shows the temperature evolution at the top and at the bottom surfaces of the blank obtained in the experimental test with a higher mould temperature of 240 °C. Figs. 18 and 19 show the comparison between the experimental and estimated values of the temperature at the

**Table 10**  
Conductance value of the contacts of the FE simulation.

Bodies in contact	Mould-Bottom Blank	Plies	Punch-Top Blank
Gap conductance [W/m <sup>2</sup> K]	2600	10,000	100

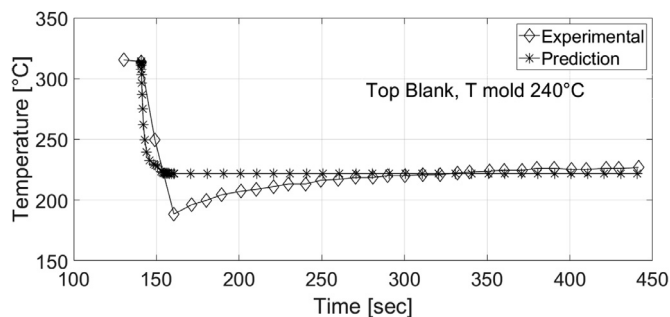


**Fig. 18.** Comparison between the experimental ( $\diamond$ ) and estimated (\*) temperature values during forming at the top of the blank; T mould 240 °C.

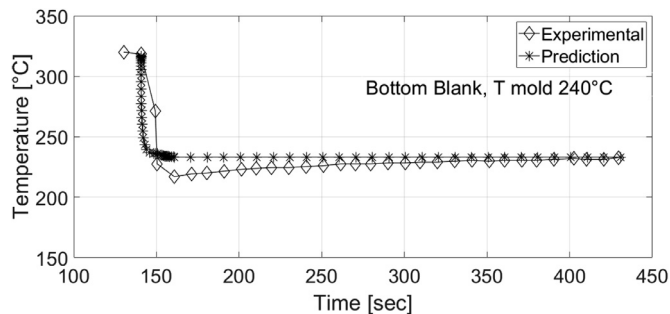


**Fig. 19.** Comparison between the experimental ( $\diamond$ ) and estimated (\*) temperature values during forming at the bottom of the blank; T mould 220 °C.

**Table 11**  
Comparison between the temperature values at the forming stage of the experimental tests and the FEA; T mould = 240 °C.

Position	Experimental T [°C]	Numerical T [°C]	Variation (%)
Top	227	221	- 2.6
Bottom	232	233	+ 0.4

top and at the bottom surfaces of the blank. The equilibrium temperatures are 227 °C and 232 °C at the surface of the top and at the bottom of the blank, respectively. A very good agreement with the experimental values is obtained, as reported in Table 11.

### 3.4. Cooling stage

Fig. 20 shows the evolution of the part spring-in (SI) angle upon cooling for the considered material and layup. The values of the spring-in angle at room temperature was 1.23°, in agreement with 1.2° reported by [11].

Results show an expected linear trend with a different slope of the SI variation occurring at the glass-transition temperature due to the variation of the  $\alpha_3$  value.

### 3.5. ANN for thermoforming of thermoplastic composites

Table 12 reports the results of the ANOM approach performed by [15].

In Table 13 the predicted values of the flexural strength based on the ANN models for the optimal process parameters (310 °C/170 °C/0.94)

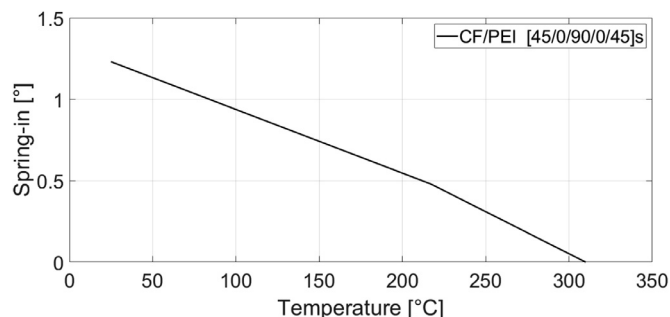


**Fig. 20.** Spring-in angle evolution upon cooling.

are listed in terms of the mean value and the standard deviation (SD). Fig. 21 offers a graphic visualization of such results compared to the ANOM value.

It can be seen that the predicted mean flexural strength values for every scenario is consistent with the ANOM value (as reported in Table 11). Focusing on the SD values, the lowest values are obtained for scenarios B, E, and H in which most of the data were devoted for the training and validation sets (70% and 25%, respectively). In terms of the effect of the number of hidden neurons a basic observation can be done by averaging the SD values for the three considered cases, i.e.  $\overline{SD}_{ABC}$ ,  $\overline{SD}_{DEF}$ ,  $\overline{SD}_{GHI}$ . Results show that the lowest average SD value is  $\overline{SD}_{DEF}$  which refers to a number of hidden neurons equal to 5. A lower SD can be interpreted as an ANN with a higher predictive performance. Hence, for HN=5 the ANN models have improved the prediction performance but for HN=10 such performance is decreased. This phenomenon is called overfitting. Determining a priori how many HN a model should have is not straightforward and ultimately it depends on the type of the analysed data. We can only conclude that for the selected scenarios the combination that offer the best predictive performance is the one with HN=5 and data allocated as 70% T, 25% V, and 5% TT, and we considered this scenario (i.e. scenario E) for the prediction of the derived production cycle and the degree of crystallinity. The results are reported in Table 14 showing a good agreement with the ANOM values shown in Table 12.

## 4. Discussion

We measured the temperature evolution during the different thermoforming stages and we investigated traditional analytical and numerical approaches as well ML-based algorithms to predict the temperature variation of the blank.

For both the heating up and the transport stages, it is crucial to mitigate the heat losses for both the heating and the transporting stages. The main parameters that have to be taken into account at the design phase are the number of plies of the blank and the convective heat transfer coefficient. We showed that for the employed setup when two more plies were added, i.e. from 2 to 4, and from 4 to 6, the time needed to reach the forming temperature increased by about 20 s. The value of the convective heat transfer coefficient was not measured but estimated and considered as a tuning parameters for the analytical investigation. A more robust estimation can be provided by its direct measurement. More importantly, the adopted analytical model is based on several assumptions that although reasonable for the considered cases, i.e. heat convection and radiation occurring only in the thickness direction in a thin laminate, they might not be suitable for a more general application.

**Table 12**  
Optimized process parameters with ANOM [15].

Optimized part characteristic	Optimal process parameters			ANOM prediction
	Blank forming temperature [ °C]	Mould tool temperature [ °C]	CCR	
Flexural strength [MPa]	310	170	0.94	979 ± 87
Derived production cycle time [s]	310	50	0.94	438 ± 15
Degree of crystallinity [%]	310	170	0.97	27.8 ± 5.3

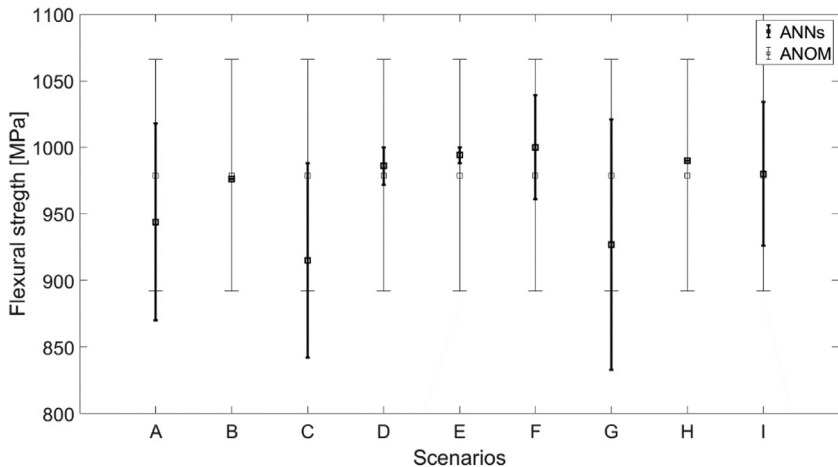


**Fig. 21.** Comparison between the flexural strengths for the optimal process parameters: ANOM vs. ANNs.

**Table 13**  
Predicted values of the flexural strengths based on the ANN models.

Scenario	Flexural Strength [MPa]
A	944 ± 74
B	976 ± 0
C	915 ± 73
D	986 ± 14
E	994 ± 6
F	1000 ± 39
G	927 ± 94
H	990 ± 0
I	980 ± 54

**Table 14**  
ANN predicted values for scenario E.

	ANN value	
Derived Production time [s]	430 ± 0	
Degree of crystallinity [%]	28.0 ± 0.4	
	ANN value	Variation ANN/ANOM (%)
Flexural strength [MPa]	994 ± 6	1.5
Derived Production time [s]	430 ± 0	1.8
Degree of crystallinity [%]	28.0 ± 0.4	0.7

Nonetheless, they provide a starting point addressing the main physical parameters involved in the thermoforming process.

The prediction of the blank temperature during forming illustrated the importance of the conductance values of the contact between the blank and the forming tools, which depends on the involved materials.

The effectiveness of the numerical model to predict the temperature of the blank during forming is strongly dependant upon the thermal contact properties. The adopted values are empirical and their order of magnitude well represent the conductivity properties of the different materials. Nonetheless, a better understanding of such properties is needed to provide a more robust formulation for different materials that might be used in the forming process, e.g. steel.

For the cooling stage, the temperature played a major role for the development of the SI angle upon cooling. The analytical predictive model we used is a Classic Laminate Theory-based analysis, valid for symmetric

lay-ups and uniform variation of temperature through the blank thickness. The model shows the importance of the variation of the stiffness and thermal properties of the polymer phase as a function of the polymer  $T_G$ .

Lastly, we applied ANNs for the evaluation of the optimum values of the process parameters to achieve maximum flexural strength, minimum derived production cycle time and maximum degree of crystallinity for the final manufactured part. The optimum values resulting from the ANN model well agree with the traditional ANOM analysis. It is important to consider that:

- In terms of the optimum processing parameters windows an approach based on ANN with respect to the traditional ANOM is not necessarily better,
- However, the ANN tool offers a higher capability to explore the whole design space to relate process parameter inputs and mechanical property outputs,
- Ultimately, the ANN tool gives the capability to provide an inline manufacturing control so that the value of multiple process parameters can continuously be fed into the ANN model to obtain a real-time prediction of the mechanical properties.
- The number of experimental data samples are very minimal and more data points are typically needed for any ML-based application. To overcome such issue in manufacturing two strategies can be implemented. The first one is based on validated FE models that can be used as data generators, while the second one is based on techniques based on virtual samples generators [43].

**5. Conclusion**

This work provides the strategy for the prediction of the temperature evolution of the blank during the thermoforming stages, i.e. heating, transporting, forming, and cooling down. The described methodologies represent an effective tool for accurate prediction of temperature especially at the initial design phase where the influence of different material, thickness, layup, and setup on the blank temperature evolution during thermoforming have to be taken into account. These factors need to be carefully considered at the initial design phase,

An optimization of the process is here proposed based on ANN models. The approach has the potential to provide good estimations of selected part characteristics as function of several process parameters. Although the application of ML-based approaches to manufacturing processes is still at an early phase, the potential are evident since predictive models can be built even if complex relationships between the process variables are unknown and then not analytically/numerically computable. This capability will enable improved design choices and inline monitoring capabilities for composites thermoforming leading to both time and material saving. Overall, it would enable the proper design of composite constituents, manufacturing processes and process parameters to obtain a specific functionality for the manufactured part. Due to the importance of the number of initial data with respect to the prediction accuracy, more research is required to solve this challenge. Promising strategies can be found both in virtual samples and in FE models as data generators.

### Declaration of Competing Interest

None.

### Acknowledgements and disclaimer

This project has received funding from the Clean Sky 2 Joint Undertaking (JU) under grant agreement No 807097. The JU receives support from the European Union's Horizon 2020 research and innovation programme and the Clean Sky 2 JU members other than the Union.

The results, opinions, conclusions, etc. presented in this work are those of the author(s) only and do not necessarily represent the position of the JU; the JU is not responsible for any use made of the information contained herein.

The authors express their gratitude to Ir. Francisco Saraiva for the experimental work conducted for his MSc degree at Delft University of Technology and upon which the results of the forming section are used in this work.

Lastly, the authors thank Mr. Fred Bosch and Mr. Victor Horbowiec from the Delft Aerospace Structures and Laboratory for their support in the development of the experimental setup.

### References

- [1] A.R. Offringa, Thermoplastic composites-rapid processing applications, *Comp. Part A* 27 (4) (1996) 329–336.
- [2] P. de Luca, P. Lefebure, A.K. Pickett, Numerical and experimental investigation of some press forming parameters of two fibre reinforced thermoplastics: APC2-AS4 and PEI-CETEX, *Comp. Part A* 29A (1998) 101–110.
- [3] J.A. Barnes, G.E. Byerly, The formation of residual stresses in laminated thermoplastic composites, *Compos. Sci. Technol.* 51 (1994) 479–494.
- [4] T.J. Chapman, J.W. Gillespie, R.B. Pipes, Prediction of process-induced residual stresses in thermoplastic composites, *J. Compos. Mater.* 24 (1990) 616–628.
- [5] A. Dutta, M. Niemeyer, M. Cakmak, Thermoforming of advanced thermoplastic composites. I: single curvature parts, *Polym. Compos.* 12 (4) (1991) 257–272.
- [6] K. Friedrich, M. Hou, On stamp forming of curved and flexible geometry components from continuous glass fiber/polypropylene composites, *Comp. Part A* 29A (1997) 217–226.
- [7] P. Han, J. Butterfield, S. Buchanan, R. McCool, Z. Jiang, M. Price, A. Murphy, The prediction of process-induced deformation in a thermoplastic composite in support of manufacturing simulation, *Proc. Inst. Mech. Eng. Part B J. Eng. Manuf.* 227 (10) (2013) 1417–1429.
- [8] Hou M., Friedrich K., “3-D stamp forming of thermoplastic matrix composites”, *applied composite materials*, 1994, 1(2), 135–153.
- [9] M. Hou, Stamp forming of fabric reinforced thermoplastic composites, *Polym. Compos.* 17 (4) (1996) 596–603.
- [10] M. Hou, Stamp forming of continuous glass fibre reinforced polypropylene, *Comp. Part A* 28 (8) (1997) 695–702.
- [11] L.K. Jain, M. Hou, L. Ye, Y.W. Mai, Spring-in study of the aileron rib manufactured from advanced thermoplastic composite, *Comp. Part A* 29A (1998) 973–979.
- [12] P.Y.B. Jar, R. Mulone, P. Davies, H.H. Kausch, A study of the effect of forming temperature on the mechanical behaviour of carbon fibre/peek composites, *Compos. Sci. Technol.* 46 (1) (1993) 7–19.
- [13] G. Jeronimidis, A.T. Parkyn, Residual stresses in carbon fibre-thermoplastic matrix laminates, *J. Comp. Mater.* 22 (1988) 401–415.
- [14] H. Lessard, G. Lebrun, A. Benkaddour, X.T. Pham, Influence of process parameters on the thermostamping of [0/90]12 carbon/polyether ether ketone laminate, *Composites: Part A* 70 (2015) 59–68.
- [15] R. McCool, A. Murphy, R. Wilson, Z. Jiang, M. Price, J. Butterfield, P. Hornsby, Thermoforming carbon fibre-reinforced thermoplastic composites, *Proc. Inst. Mech. Eng. Part L J. Mater. Des. Appl.* 226 (2011) 91–102.
- [16] C.M. O’Bradaigh, P.J. Mallon, Effect of forming temperature on the properties of polymeric diaphragm formed thermoplastic composites, *Compos. Sci. Technol.* 35 (3) (1989) 235–255.
- [17] D. Tatsuno, T. Yoneyama, K. Kawamoto, M. Okamoto, Effect of side die pressure and adaptive die temperature control in press forming of U-beam using carbon fiber-reinforced PA sheets, *J. Comp. Mater.* 51 (30) (2017) 4273–4286.
- [18] W.J. Unger, J.S. Hansen, The effect of cooling rate and annealing on residual stress development in graphite fibre reinforced PEEK laminates, *J. Comp. Mater.* 27 (1993) 108–130.
- [19] R. Akkerman, B. Rietman, S. Haanappel, U. Sachs, Towards design for thermoplastic composites manufacturing using process simulation, in: *Proceedings of International Conference and Exhibition on Thermoplastic Composites*, 2012.
- [20] R. Akkerman, S.P. Haanappel, U. Sachs, History and future of composites forming analysis, in: *13th International Conference on Textile Composites (TEXCOMP-13)*, 2018, p. 406. IOP Conf. Series: Materials Science and Engineering.
- [21] P. Bussetta, N. Correia, Numerical forming of continuous fibre reinforced composite material: a review, *Composites: Part A* 113 (2018) 12–31.
- [22] Y.K. Hamidi, A. Berrado, M. Cengiz Altan, Machine learning applications in polymer composites, in: *AIP Congerence Proceedings*, 2020, p. 2205.
- [23] A.G. Stamopoulos, K.I. Tserpes, A.J. Dentsoras, Quality assessment of porous CFRP specimens using X-ray computed tomography data and artificial neural networks, *Compos. Struct.* 192 (2018) 327–335.
- [24] B. Denizer, Artificial neural network analysis of the mechanical properties of tungsten fiber/bulk metallic glass matrix composites via neutron diffraction and finite element modelling”, *Graduate Dissertation*, Iowa State University, 2008.
- [25] G. Balokas, S. Czichon, R. Rolfes, Neural network assisted multiscale analysis for the elastic properties prediction of 3D braided composites under uncertainty, *Compos. Struct.* 183 (1) (2018) 550–562.
- [26] R. Haj-Ali, H.K. Kim, Nonlinear constitutive models for FRP composites using artificial neural network, *Mech. Mater.* 39 (2007) 1035–1042 39.
- [27] Z. Zhang, K. Friedrich, Artificial neural networks applied on polymers and composites: a review, *Compos. Sci. Technol.* 63 (2003) 2029–2044.
- [28] F. Saraiva, Development of press forming techniques for thermoplastic composites – Investigation of a multiple step forming approach, *MSc Dissertation*, Delft University of Technology, 2017.
- [29] S. Hu, J.A. Nairn, On the thermally-induced residual stresses in thick fiber-thermoplastic matrix (PEEK) cross-ply laminated plates, *NASA Technical Documents*, 1992.
- [30] F.P. Incropera, D.P. De Witt, T.L. Bergman, A.S. Lavine, *Fundamentals of Heat and Mass Transfer*, 6th Ed., Wiley, 2012.
- [31] H. Shi, I.F. Villegas, H.E.N. Bersee, A study of process induced voids in resistance welding of thermoplastic composites, *20th International Conference on Composite Materials*, 2015.
- [32] Toray Cetex TC 1000 Premium PEI Datasheet, <https://www.toraytac.com/product-explorer/products/uHNz/Toray-Cetex-TC1000-Premium>.
- [33] N.P. Anbuehzhian, Research on the process window for multi-step forming of CF/PA12 composite prepreg”, *MSc Dissertation*, Delft University of Technology, 2017.
- [34] M.D. Wakeman, L. Zingraff, P.E. Bourban, J.A.E. Manson, P. Blanchard, Stamp forming of carbon fibre/PA12 composites – a comparison of a reactive impregnation process and a commingles yarn system, *Compos. Sci. Technol.* 66 (2006) 19–35.
- [35] *Matweb Datasheet*, 2021 <http://www.matweb.com/search/datasheet.aspx?matguid=0e37a459c4eb452faa9d92659f9a0ccc>.
- [36] Torayca, T300 Datasheet, 2021 <https://www.fibermaxcomposites.com/shop/datasheets/T300.pdf>.
- [37] FESTO, 2021 [https://www.festo.com/cat/nl\\_nl/data/doc\\_engb/PDF/EN/DSBC\\_EN.PDF](https://www.festo.com/cat/nl_nl/data/doc_engb/PDF/EN/DSBC_EN.PDF).
- [38] ABAQUS Documentation, 2021 <https://abaqus-docs.mit.edu/2017/English/SIMACAEITNRefMap/simaitn-c-thermalinteraction.htm>.
- [39] L.P. Kollar, Approximate analysis of the temperature induced stresses and deformations of composite shells, *J. Compos. Mater.* 28 (5) (1994) 392–423.
- [40] A.A. Fahmy, A.N. Ragai-Ellozy, Thermal expansion of laminated fiber composites in the thickness direction, *J. Compos. Mater.* 8 (1973) 90–92.
- [41] N.J. Pagano, Thickness expansion coefficients of composite laminates, *J. Compos. Mater.* 8 (1974) 310–312.
- [42] K.M. Saridakis, A.C. Chasalevris, C.A. Papadopoulos, A.J. Dentsoras, Applying neural networks, genetic algorithms and fuzzy logic for the identification of cracks in shafts by using coupled response measurements, *Comput. Struct.* 86 (2008) 1318–1338.
- [43] C. Wanigasekara, E. Oromiehie, A. Swain, Gangadhara Prusty, S.K. Nguang, Machine learning based predictive model for AFP-based unidirectional composite laminates, *IEEE Trans. Ind. Inf.* 16 (2020) 2315–2323.